Solvothermal synthesis of high-performance Ni-Co layered double hydroxide nanofoam electrode for electrochemical energy storage

Rajkumar Patel[a,*], Akbar I. Inamdar[a, *], Bo Hou[b], SeungNam Cha[b], Abu Talha Ansari[a], Jayavant L. Gunjakar[a], Hyunsik Im[a,*], Hyungsang Kim[a,*]

[a] *Division of Physics and Semiconductor Science, Dongguk University, Seoul 04620, Korea*

[b] *Department of Engineering Science, University of Oxford, Parks Road, OX1 3PJ, UK*

[*]Corresponding Authors:
Email: patelrajku@gmail.com (R. Patel), akbarphysics2002@gmail.com (A.I. Inamdar), hyunsik7@dongguk.edu (H. Im) and hskim@dongguk.edu (H. Kim).

Abstract

A nanofoam nickel cobalt hydroxide ($NiCo(OH)_2$) electrode film is fabricated on a stainless-steel substrate with the use of a simple one-step solvothermal process. The nanofoam NiCo(OH)2 electrode exhibits a high specific capacitance of 2710.2 F/g at a current density of 9.1 A/g, and a good capacity retention of ~ 70 % after 2000 charge-discharge cycles at a high current density of 31.8 A/g. An energy density of 60.23 Wh/kg is obtained at a power density of 1.8 kW/kg. The excellent electrochemical energy storage performance of the $NiCo(OH)_2$ electrode is due to the synergetic effect of a significantly improved ionic diffusion and an effective charge transfer, which is linked to a well-dispersed interconnected nanofoam morphology and binder-free direct contact with the current collector.

Keywords: Solvothermal process, nickel cobalt hydroxide, nanofoam structure, electrochemical properties

1. Introduction

As the demand for advanced electronic devices that require higher power and energy densities continues to rapidly increase, the ongoing development of rechargeable high-performance power sources is indispensable. Supercapacitors that are intermediate in terms of the energy and power densities between the conventional capacitors and batteries have attracted considerable attention due to a fast charge rate, long-cycle life, excellent stability, and safety. Supercapacitors are, generally, categorized into the following two types depending on the used electrode materials: carbon-based electrical double-layer capacitors (EDLCs), and pseudo-capacitors that are based on metal oxides (or hydroxide) such as NiO, Co_3O_4, MnO_2, RuO_2, $Ni(OH)_2$, and $Co(OH)_2$[1,2,3,4,5,6,7]. Although carbon-based ELDCs have a high power density, they are lacking in terms of the specific capacitance and energy density. Alternatively, it is anticipated that metal-oxide and hydroxide compounds have a higher specific capacitance and energy density due to the interfacial redox reaction and the multiple valence states of the metal ions. However, the properties of mono oxides/hydroxides like NiO, Co_3O_4, MnO_2, $Ni(OH)_2$, and $Co(OH)_2$ have a lower specific capacitance due to either a low conductivity or a poor redox behavior. Despite its high performance, ruthenium is a rare-earth element, meaning that the cost of RuO_2 is higher and its applications are therefore limited[8,9,10,11].

The mixed-metal nanostructure oxides (or hydroxides) whose constituting elements are Earth-abundant are likely to exhibit improved electrochemical properties as regarding their electrodes due to the combination of capacitive and conductive behaviors, and the corresponding synergetic effect of the different metal ions keeps the material costs low. Nickel cobalt layered double hydroxide is one of the promising electrode materials due to its high theoretical-capacitance value of > 3000 F/g, a superior redox activity, and because it is an economical as

well as an environmentally friendly chemical.[12] It is generally difficult, however, to optimize the compositional ratio and morphology of binary metal hydroxides using a simple fabrication technique. Additionally, because of several advantages, the binder-free direct-growth of electrode materials is desirable. A number of methods are often used to directly grow an active material on a substrate such as the hydrothermal method, chemical-bath deposition, potentiostatic deposition, pulsed-laser deposition, thermal transformation, and the post-annealing and sputtering method[13,14,15,16,17,18,19]. The hydrothermal method is especially efficient for the preparation of layered double hydroxide (LDH) materials and is simpler than the other methods[20,21] In this work, nickel-cobalt-layered double hydroxide ($NiCo(OH)_2$) was grown directly on a stainless-steel (SS) substrate by using a simple facile, one-step hydrothermal method under the solvothermal condition. The electrochemical measurement reveals the highest specific capacitance of 2712.2 F/g at a current density of 9.1 A/g; furthermore it shows a good capacity retention of 67.8 % after 2000 cycles at a high current density of 31.8 A/g.

2. Experimental

2.1. $NiCo(OH)_2$ synthesis

The $NiCo(OH)_2$ electrode films were fabricated using a solvothermal process. The nickel chloride hexahydrate ($NiCl_2.6H_2O$) and the cobalt chloride hexahydrate ($CoCl_2{\cdot}6H_2O$) are the sources of the nickel and cobalt, respectively, in the $NiCo(OH)_2$. The molar ratio of the $NiCl_2{\cdot}6H_2O$: $CoCl_2{\cdot}6H_2O$: urea combination is maintained at 2.76:4.98:7.49, and it was dissolved in methanol. The washed SS substrate was placed into the autoclave along with the precursor solution, and after it was sealed, the temperature of the oven was maintained at 110 ^oC for 12 h. The electrode with $NiCo(OH)_2$ was then washed with methanol and water to remove the

weakly bound residual products, followed by a drying at 60 ^{o}C. The weight of the $NiCo(OH)_2$ film is accurately calculated by the measuring of the difference between the weights of the pristine substrate and the electrode coated with the $NiCo(OH)_2$ film.

2.2. Physical characterization and electrochemical measurements

The microstructure of the $NiCo(OH)_2$ electrode film and its structural-phase change after the electrochemical measurements were determined via transmission electron microscopy (TEM, JEOL 2010) and selected area electron diffraction (SAED), respectively. The acceleration voltage was set as 200 kV. The crystallinity of the $NiCo(OH)_2$ film was measured using X-ray diffraction (XRD; Rigaku, Smart Lab) with a cathode operating at 40 kV and 30 mA. The range of the 2θ angular regions is between 5^{o} and 80^{o}, and the measurement was performed at a scan rate of 2^{o}/min. The surface morphology was measured using field-emission scanning electron microscopy (FE-SEM; SUPRA 55VP, Carl Zeiss, Germany) operating at 15 kV. The supercapacitance behavior of the $NiCo(OH)_2$ film was studied using a conventional three-electrode cell in 1 M aqueous KOH solution; here, the $NiCo(OH)_2$ is the working electrode, while the saturated calomel electrode (SCE) served as the reference electrode and the Pt rod functioned as the counter electrode. A potentiostat (Princeton Applied Research, VersaSTAT 3) was used to measure the cyclic voltammetry (CV). The galvanometric-charge/discharge test was performed with the use of the potentiostat/galvanostat in the galvanostatic mode. An impedance analyzer was used to carry out the electrochemical impedance spectroscopy (EIS).

3. Results and discussion

Figure 1 (a) represents the schematic representation of the synthesis of the $NiCo(OH)_2$. Under a mild solvothermal condition, the rate of the release of the hydroxyl anion is moderate, leading to a controlled reaction with the metal-amine complex that induces a well-developed nanoform like morphology of binary-layer double hydroxide that is described as follows;

$$Ni(NH_3)_4^{2+} + 2OH^- \longrightarrow Ni(OH)_2 + 4NH_3 \quad (1)$$

$$Co(NH_3)_4^{2+} + 2OH^- \longrightarrow Co(OH)_2 + 4\ NH_3 \quad (2)$$

The chloride ion in the reaction media is intercalated in the layered $NiCo(OH)_2$, and it is replaced with hydration and exchanged by the hydroxyl anion present in the aqueous electrolyte during the electrochemical performance measurement. Figure 1 (b) represents the XRD pattern of the as-prepared $NiCo(OH)_2$ film on the SS substrate. The sharp peaks denoted by the asterisk (*) symbol are due to the SS substrate. The XRD diffraction peaks that appear at the 2θ value of 11.42^o, 23.1^o, 33.58^o, 57.64^o, and 58.82^o, correspond to the (003), (006), (012), (110), and (113) planes of the reflections of $NiCo(OH)_2$ respectively; here, it is indexed as both α-$Ni(OH)_2$ (JCPD: 38-0715) and α-$Co(OH)_2$ (JCPD: 46-0605). Because the sizes of Ni and Co ions are almost similar, they can replace each other in the crystalline sites of $NiCo(OH)_2$[22,23]. The elemental analysis from the energy dispersive X-ray spectroscopy (EDX) measurement is presented in Figure 1 (c). The ratio of Ni to Co in terms of the atomic percent is approximately 1.46:1.51. The atomic percent of the chloride present in the nanofoam film is 18.44 %. The chloride anion is intercalated within the interlayer space offered by the $NiCo(OH)_2$ host, along with water molecules. The morphology of the LDH film was studied using FE-SEM, and as presented in Fig. 1 (d), the $NiCo(OH)_2$ LDH film has a nanofoam morphology. The dissolution-recrystallization process is the pathway for the nanofoam-like morphology of $NiCo(OH)_2$[24]. The

flakes in the nanofoam are well interconnected with each other, forming a network-like structure with a large surface area, and because they are also well attached to the SS substrate, they provide excellent electron-diffusion paths. The wall thickness of the nanofoam is approximately 10 nm. The foam-like morphology is favorable for the electrochemical energy-storage performance due to the larger inter-sheet space that results in a more-effective ionic diffusion. The microscopic structure of the $NiCo(OH)_2$ sample was revealed using TEM and high-resolution (HR)-TEM, as shown in Figs. 1 (e) and (f), respectively; here the nanofoam morphology of the sample is clearly visible in the TEM image. The long-range ordered structure of the nanofoam morphology is indicated by the sharp diffraction spots and rings of the SAED pattern. The lattice fringes of 0.47 nm and 0.24 nm in the HR-TEM image corresponds to the (006) and (110) crystal faces, respectively, of the hydrotalcite-like LDH structure[12].

Figure 2 (a) shows the CV curves that were measured at different scan rates. The redox peak observed in the CV curves indicates that the binary metal hydroxide showed the pseudo-capacitance behavior. The oxidation and reduction peaks are evident at 0.31 V and 0.13 V, respectively, at a scan rate of 5 mV/s. The small potential-difference value is indicative of a sound reversibility of the electrochemical reactions. The faradic reactions of the $NiCo(OH)_2$ electrode in the alkaline KOH electrolyte are described by the following equations[25,26]:

$$Ni(OH)_2 + OH^- \rightleftharpoons NiOOH + H_2O + e^- \quad (3)$$

$$Co(OH)_2 + OH^- \rightleftharpoons CoOOH + H_2O + e^- \quad (4)$$

The oxidation process of the metal hydroxides produces metal oxyhydroxide species that show the pseudo-capacitive behavior. We have not observed individual oxidation and reduction peaks

of nickel hydroxide and cobalt hydroxide. This is presumably due to the similar oxidation and reduction behaviors of nickel hydroxide and cobalt hydroxide [25,26].

Figure 2 (b) shows the galvanostatic charge/discharge characteristics of the $NiCo(OH)_2$ electrode at different current densities. The shape of the charge-discharge curve is typical of pseudo-capacitors. The IR drop is ~ 50 mV at a current density of 9.1 A/g, indicating a low internal resistance at the electrode/electrolyte interface. The highest specific capacitance of 2710.2 F/g is obtained at the lowest current density of 9.1 A/g (Fig. 2 (c)). The calculated capacitance values are considerably higher than the previously reported ones that were obtained from $NiCo(OH)_2$ electrodes with different nano-morphologies and intercalated anions[27,28]. This difference is presumably because the well-dispersed nanofoam structure of the electrode allows the penetration of the ion towards the inner core of the electrode, thereby enhancing the faradic reaction. Metal hydroxides that were intercalated with different anions such as chloride (Cl^-), nitrate (NO_3^-), acetate (CH_3COO^-), and sulfate (SO_4^-) were synthesized, and it was found that the metal hydroxides intercalated with the chloride anion showed the highest capacitance value; this is because the size of the chloride anion is the smallest, thereby enhancing the hydroxyl anion mobility[29,30]. Accordingly, the small-sized singly-charged chloride ions in $NiCo(OH)_2$ exchanged efficiently with the hydroxyl anion, leading to a higher specific capacitance. In addition, the obtained capacitance value (~2710 F/g at 9.1 A/g) of the $NiCo(OH)_2$ LDH electrode is considerably higher than those of three-dimensional nanoporous $Ni(OH)_2$ (~1519 F/g at 7A/g)[31], nanostructured $Ni(OH)_2$ (~1025 F/g at 1A/g)[32], $Co(OH)_2$ nanosheets (~1164 F/g at 1A/g)[33] and $Co(OH)_2$ rods (~1116 F/g) [34].

Fig. 3(a) shows the CV cathodic peak current density as a function of square root of scan rate ($v^{1/2}$) for various LDH materials[11,30,35,36]. The peak current increases linearly with $v^{1/2}$ and this is due to the diffusion-controlled reaction of hydroxyl ions. The relative diffusion coefficient (DR) can be calculated from the following equation[37];

$$D_R = \left\{ \left(j_p / v^{1/2} \right) / \left(j_p / v^{1/2} \right)_{Ref} \right\}^2 \quad (5)$$

where j_p represents the cathodic peak current density. Table 1 compares the calculated relative diffusion coefficient of our electrode with some other LDH electrodes[11,30,35,36]. The larger diffusion coefficient value of our sample reveals that it has improved interlayer spacing by the intercalation of the chloride ion. The performance of the electrode is dependent on the electrochemically active surface area (ECSA). It is measured in the non-Faradic low voltage linear-charging region below 0.25 V in which the current is proportional to the scan rate v as follows[38];

$$i_{DL} = C_{DL} v \quad (6)$$

$$ECSA = C_{DL}/C_S \quad (7)$$

where i_{DL} represents the current on the non-Faradaic linear charging region, C_{DL} is the linear region capacitance, and C_S is the capacitance of the KOH electrolyte. Here, Cs =0.04 mF/m^2 [39]. The C_{DL} value was estimated using the corresponding current density at 50 mV/s (see Fig. 3(b)). The obtained ECSA value for our sample is found to be 3632 cm^{-2} which results in better electrochemical performance. Recently, Kannan et al. reported an ECSA value of 496 cm^{-2} for a nanostructured nickel oxide electrode film[38].

Based on the charge-discharge measurements, the energy density and the power density (Ragone plot) for the $NiCo(OH)_2$ electrode were obtained, as shown in Fig. 4 (a); subsequently,

excellent power and energy densities were obtained. Fig. 4 (b) presents the capacity retention of the $NiCo(OH)_2$ nanofoam electrode up to 2000 charge-discharge cycles at a current density of 31.8 A/g and a 67.8 % capacity retention is shown after 2000 cycles. The inset represents the morphology of the electrode after the stability test. The repeated intercalation/deinercalation processes of the hydroxyl ions produce in-plain strain-generating cracks in the surface of the electrode[31]. Figure 4 (c) presents the electrochemical-impedance spectra of the electrode before and after the cycling in the frequency range of 10^4 Hz to 10^{-2} Hz. The spectra consist of three elements, as follows: solution resistance (R_S), charge-transfer resistance (R_{ct}) at the electrolyte/electrode interface (semicircle in the high-frequency region), and the Warburg impedance (Z_W) that corresponds to the straight line in the low-frequency region. After the cycling test, the R_{ct} and Z_W increased from 1.39 Ω to 18.07 Ω and from 2.65 Ω to 2.92 Ω, respectively. Extracted parameter values of the equivalent circuit are presented in Table 2.

4. Conclusions

For this work, a binder-free $NiCo(OH)_2$ electrode is successfully synthesized on an SS substrate through the use of a simple template-free solvothermal process. The electrode has a well-interconnected nanofoam morphology intercalated with chloride anions, and it exhibits a maximum specific capacitance of 2710.2 F/g at a current density of 9.1 A/g. A sound capacitive retention of ~ 70 % after 2000 cycles was observed at ~ 32 A/g; furthermore, high power and energy densities were obtained. The excellent electrochemical energy-storage properties of the $NiCo(OH)_2$ electrode are due to the synergetic effect between a large specific-surface area, binder-free direct contact between the electrode and the current collector with a low resistance,

and an improved ionic diffusion of the electrolyte that is due to the intercalated chloride anion that is induced by a large inter-gallery spacing.

5. Materials and methods

5.1. $NiCo(OH)_2$ synthesis

The $NiCo(OH)_2$ electrode films were fabricated using a solvothermal process. The nickel chloride hexahydrate ($NiCl_2 \cdot 6H_2O$) and the cobalt chloride hexahydrate ($CoCl_2 \cdot 6H_2O$) are the sources of the nickel and cobalt, respectively, in the $NiCo(OH)_2$. The molar ratio of the $NiCl_2 \cdot 6H_2O$:$CoCl_2 \cdot 6H_2O$:urea combination is maintained at 2.76:4.98:7.49, and it was dissolved in methanol. The washed SS substrate was placed into the autoclave along with the precursor solution, and after it was sealed, the temperature of the oven was maintained at 110 ^oC for 12 h. The electrode with $NiCo(OH)_2$ was then washed with methanol and water to remove the weakly bound residual products, followed by a drying at 60 ^oC. The weight of the NiCo(OH)2 film is accurately calculated by the measuring of the difference between the weights of the pristine substrate and the electrode coated with the $NiCo(OH)_2$ film.

5.2. Physical characterization and electrochemical measurements

The microstructure of the $NiCo(OH)_2$ electrode film and its structural-phase change after the electrochemical measurements were determined via transmission electron microscopy (TEM, JEOL 2010) and selected area electron diffraction (SAED), respectively. The acceleration voltage was set as 200 kV. The crystallinity of the $NiCo(OH)_2$ filmwas measured using X-ray diffraction (XRD; Rigaku, Smart Lab) with a cathode operating at 40 kV and 30 mA. The range

of the 2q angular regions is between 5^{o} and 80^{o}, and the measurement was performed at a scan rate of 2^{o}/min. The surface morphology was measured using field-emission scanning electron microscopy (FE-SEM; SUPRA 55VP, Carl Zeiss, Germany) operating at 15 kV. The supercapacitance behavior of the $NiCo(OH)_2$ film was studied using a conventional three-electrode cell in 1 M aqueous KOH solution; here, the $NiCo(OH)_2$ is the working electrode, while the saturated calomel electrode (SCE) served as the reference electrode and the Pt rod functioned as the counter electrode. A potentiostat (Princeton Applied Research, VersaSTAT 3) was used to measure the cyclic voltammetry (CV). The galvanometric-charge/discharge test was performed with the use of the potentiostat/galvanostat in the galvanostatic mode. An impedance analyzer was used to carry out the electrochemical impedance spectroscopy (EIS).

Acknowledgments

The research was supported by the National research Foundation of Korea (2015M2A2A6A02045252, 2015R1D1A1A01058851, 2015R1D1A1A01060743, 2015R1A2A2A01004782 and 2016R1A6A1A03012877).

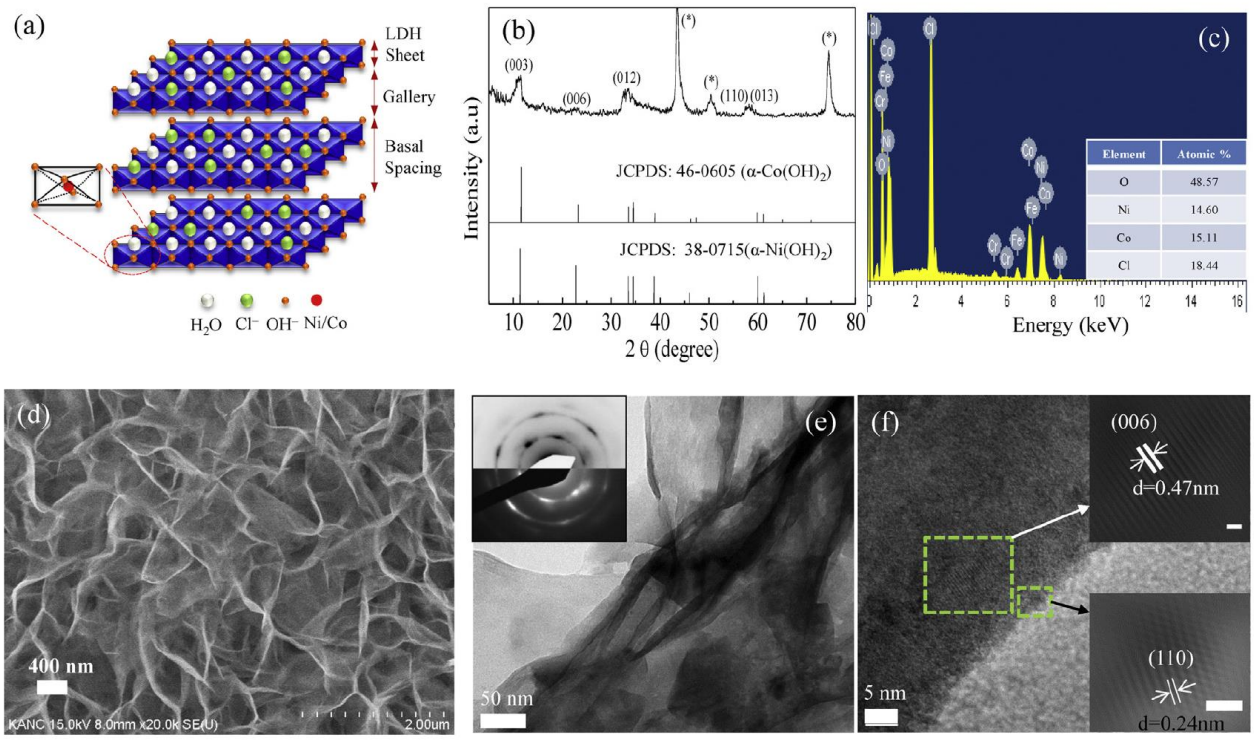

Fig. 1. (a) Pictorial representation of the synthesis and the $NiCo(OH)_2$ intercalated with chloride (Cl^-) ions, (b) XRD pattern of $NiCo(OH)_2$ film on a stainless-steel substrate, (c) energy dispersive X-ray analysis of $NiCo(OH)_2$ and the atomic percentages of the main constituting elements, (d) SEM image of $NiCo(OH)_2$, (e) TEM image of $NiCo(OH)_2$ (inset: SAED pattern), and (f) high-resolution TEM image of $NiCo(OH)_2$.

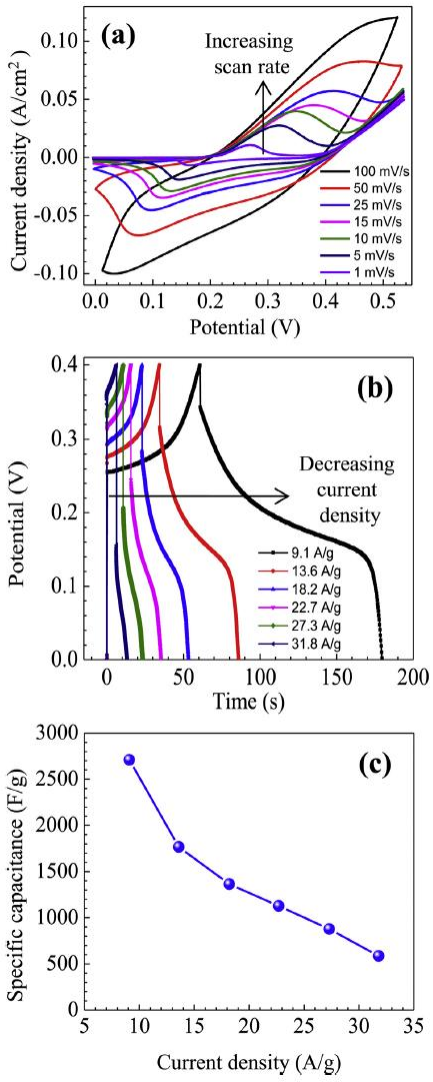

Fig. 2. (a) CV curves of the $NiCo(OH)_2$ electrode at different scan rates, (b) galvanostatic charge/discharge curves of the $NiCo(OH)_2$ electrode at different current densities, and (c) specific capacitance as a function of the current density.

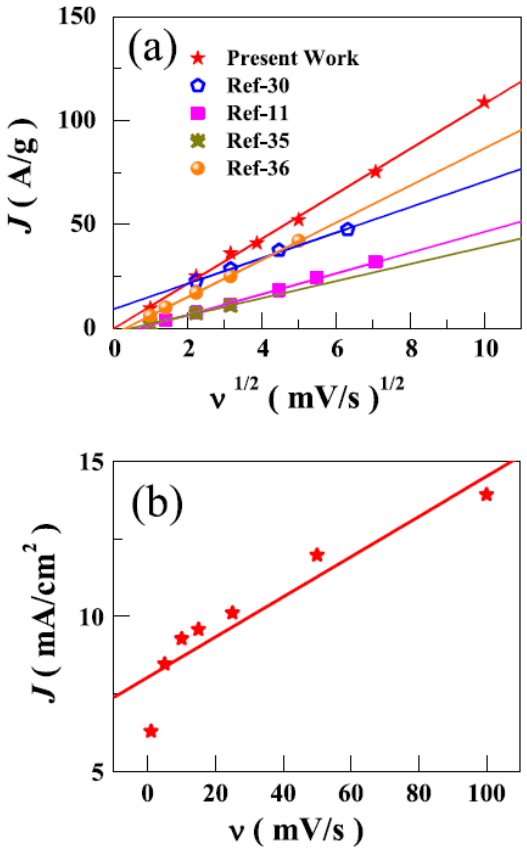

Fig. 3. (a) Cathodic peak current density versus square root of scan rate for our sample and other LDH electrodes, (b) current density versus scan rate extracted from the nonlinear region of the CV curves at 0.24 V. The extracted ECSA value is ~3632 cm^{-2}.

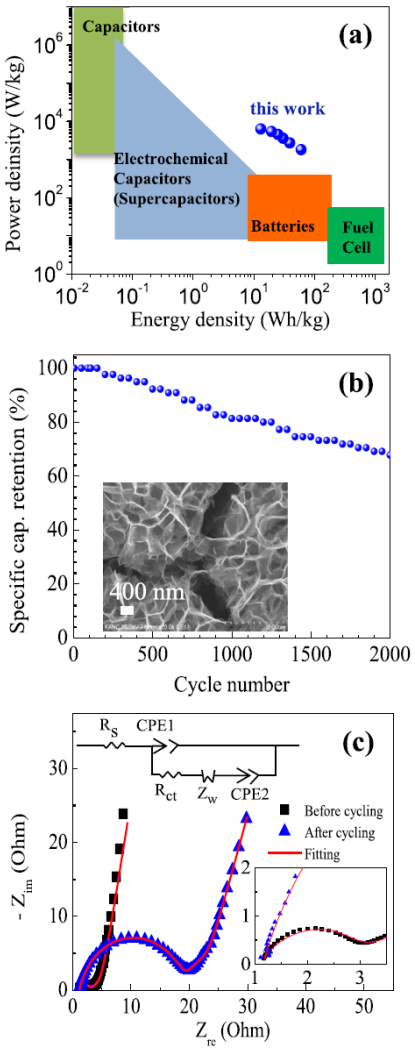

Fig. 4. (a) Ragone plot showing energy density and power density, (b) cycling performance of $NiCo(OH)_2$ at a current density of 31.8 A/g for 2000 charge/discharge cycles (inset: morphology of $NiCo(OH)_2$ after 2000 cycles), and (c) Nyquist plots of the $NiCo(OH)_2$ electrode before the first discharge cycle and after the 2000^{th} charge-discharge cycle. The inset shows an equivalent-circuit diagram for the modeling of the measured impedance curves.

Table 1

Calculated relative diffusion coefficient of our sample and other LDH electrodes.

LDH materials	$J(A/g)@v^{1/2}$ = 8 mv/s	Relative diffusion coefficient (D_R)
NiCo(OH)2, Present work	86.32	1
Ni(OH)2, ref.11	36.36	5.63
NiCo LDH, ref.30	58.27	2.19
NiCo LDH, ref.35	30.90	7.80
$Ni(Co(OH)_2CO_3$, ref. 36	68.64	1.58

Table 2

Main parameter values from the EIS measurements before and after cycling.

	R_s (Ω)	R_{ct} (Ω)	CPE-1	Zw (Ω)	CPE-2
Before cycling	1.146	1.39	$5.2*10^{-4}$	2.652	0.35
Ni(OH)2, ref.11	1.149	18.07	$6.8*10^{-4}$	2.921	0.25

References

[1] X.Y. Lang, A. Hirata, T. Fujita, M.W. Chen, Nat. Nanotechnol 6 (2011) 232-236.

[2] J. Jiang, Y. Li, J. Liu, X. Huang, C. Yuan, X. Lou, Adv. Mater. 24 (2012) 5166-5180.

[3] C. Yuan, L. Yang, L. Hou , L. Shen , X. Zhang , X.W. Lou, Energy Environ. Sci., 5 (2012) 7883-7887.

[4] R. Liang, G. Wang, X. Huang, L. Zhu, S. Li, Y. Yan, B. Zhong, Materials Letters158(2015)128–131.

[5] S.H. Kazemi, A. Asghari , Materials Letters142(2015)156–159

[6] J. He, Y. Zhao, D-B. Xiong, W. Ran, J. Xu, Y. Ren, L. Zhang, Y. Tang, F. Gao, Materials Letters, 128 (2014) 117–120.

[7] S. Ren, C. Yang, C. Sun, Y. Hui, Z. Dong, J. Wang, X. Su, Materials Letters 80 (2012) 23–25.

[8] M. Hsu, C. Chang, H. Weng, ACS Sustain. Chem. Eng. 4 (2016) 1381-1391.

[9] X. Wang, X. Han, M. Lim, N. Singh, C.L. Gan, M. Jan, P.S. Lee, J. Phys. Chem. C 116 (2012) 12448-12454.

[10] Z. Li, G. Liu, Y. Zhang, Y. Zhou, Y. Yang, Materials Research Bulletin 80 (2016) 191-199.

[11] C. Wang, X. Zhang, X. Sun, Y. Ma, Electrochimica Acta 191 (2016) 329-336.

[12] T. Li, G.H. Li, L.H. Li, L. Liu, Y. Xu, H.Y. Ding, T. Zhang, ACS Appl. Mater. Interfaces 8 (2016) 2562-2572.

[13] A.I. Inamdar, Y. Jo, J. Kim, J. Han, S.M. Pawar, R.S. Kalubarme, C.J. Park, J.P. Hong, Y.S. Park, W. Jung, H. Kim, H. Im, Energy 83 (2015) 532-538.

[14] S.M. Pawar, J. Kim, A.I. Inamdar, H. Woo, Y. Jo, B.S. Pawar, S. Cho, H. Kim, H. Im, Scientific Reports**,** DOI: 10.1038/srep21310.

[15] S.M. Pawar, A.I. Inamdar, K.V. Gurav, Y. Jo, H. Kim, J.H. Kim, H. Im, Materials Letters 141 (2015) 336-339.

[16] G.Q. Zhang, H.B. Wu, H.E. Hoster, M.B. Chan-Park, X.W. Lou, Energy Environ. Sci. 5 (2012) 9453-9456.

[17] Y. Yu, W. Zeng, H. Zhang, Hydrothermal synthesis of assembled WO3·H2O nanoflowers with enhanced gas sensing performance, Mater. Lett. 171 (2016)162-165.

[18]T. Han, Z. Zhang, Novel hydrolyzing synthesis of CeO2eRGO support for Pt electrocatalyst in direct methanol fuel cells, Mater. Lett. 154 (2015) 177-179.

[19]R. Patel, A.I. Inamdar, H.B. Kim, H. Im, H. Kim, In-Situ hydrothermal synthesis of a MoS_2 nanosheet electrode for electrochemical energy storage applications, J. Korean Phys. Soc. 68 (2016) 1341-1346.

[20]M.D. Arco, R. Trujillano, V. Rives, Cobalteiron hydroxycarbonates and their evolution to mixed oxides with spinel structure, J. Mater. Chem. 8 (1998) 761-767.

[21]R. Ma, Z. Liu, K. Takada, N. Iyi, Y. Bando, T. Sasaki, Synthesis and exfoliation of Co^{2+}-Fe^{3+} layered double hydroxides: an innovative topochemical approach, J. Am. Chem. Soc. 129 (2007) 5257-5263.

[22]R. Valdez, D.B. Grotjahn, D.K. Smith, J.M. Quintana, A. Olivas, Nanosheets of Co-(Ni and Fe) layered double hydroxides for electrocatalytic water oxidation reaction, Int. J. Electrochem. Sci. 10 (2015) 909-918.

[23]V. Gupta, S. Gupta, N. Miura, J. Power Sources 175 (2008) 680-685.

[24]K. He, G. Zhao, G. Han, CrystEngComm 16 (2014) 11050-11057.

[25]G. Chen, S.S. Liawa, B. Li, Y. Xua, M. Dunwell, S. Deng, H. Fan, H. Luo, J. Power Sources 251 (2014) 338-343

[26]C. Shang, S. Dong, S. Wang, D. Xiao, P. Han, X. Wang, L. Gu, G. Cui, ACS Nano 7 (2013) 5430-5436.

[27]M. Wang, J. Xue, F. Zhang, W. Ma, H. Cui, J. Nanopart. Res. 17 (2015) 106.

[28]J. Li, M. Yang, J. Wei, Z. Zhou, Nanoscale, 4 (2012) 4498-4503

[29]Z-A. Hu, Y-L. Xie, Y-X. Wang, L-J Xie, G-R Fu, X-Q Jin, Z-Y Zhang, Y-Y Yang, H-Y Wu, J. Phys. Chem. C 113 (2009) 12502-12508

[30]J.W. Lee, J.M. Ko, J-D Kim, J. Phys. Chem. C 115 (2011) 19445-19454.

[31]Y. Yang, L. Li, G. Ruan, H. Fei, C. Xiang, X. Fan, J.M. Tour, Hydrothermally formed three-dimensional nanoporous $Ni(OH)_2$ thin-film supercapacitors, ACS Nano 8 (2014) 9622-9628.

[32]X. Zhou, D. Cao, J. Huang, K. Ye, S. Yang, T. Liu, X. Liu, J. Yin, G. Wang, Capacitance performance of nanostructured b-$Ni(OH)_2$ with different morphologies grown on nickel foam, J. Electroanal. Chem. 720-721 (2014) 115-120.

[33]A.A.M. Barmi, M. Aghazadeh, B. Arhami, H.M. Shiri, A.A. Fazl, E. Jangju, Porous cobalt hydroxide nanosheets with excellent supercapacitive behavior, Chem. Phys. Lett. 541 (2012) 65-69.

[34]R.R. Salunkhe, B.P. Bastakoti, C.-T. Hsu, N. Suzuki, J.H. Kim, S.X. Dou, C.-C. Hu, Y. Yamauchi, Direct growth of cobalt hydroxide rods on nickel foam and its application for energy storage, Chem. Eur. J. 20 (2014) 3084-3088.

[35]W. Zhu, Z. Lu, G. Zhang, X. Lei, Z. Chang, J. Liu, X. Sun, Hierarchical $Ni_{0.25}Co_{0.75}(OH)_2$ nanoarrays for a high-performance supercapacitor electrode prepared by an in situ conversion process, J. Mater. Chem. A 1 (2013) 8327-8331.

[36]Y. Tang, Y. Liu, S. Yu, W. Guo, S. Mub, H. Wang, Y. Zhao, L. Hou, Y. Fan, F. Gao, Template-free hydrothermal synthesis of nickel cobalt hydroxide nanoflowers with high performance for asymmetric supercapacitor, Electrochim. Acta 161 (2015) 279-289.

[37]S. Liu, K.S. Hui, K.N. Hui, Flower-like copper cobaltite nanosheets on graphite paper as high-performance supercapacitor electrodes and enzymeless glucose sensors, ACS Appl. Mater. Interfaces 8 (2016) 3258-3267.

[38]V. Kannan, A.I. Inamdar, S.M. Pawar, H.-S. Kim, H.-C. Park, H. Kim, H. Im, Y.S. Chae, Facile route to NiO nanostructured electrode grown by oblique angle deposition technique for supercapacitors, ACS Appl. Mater. Interfaces 8 (2016) 17220-17225.

[39]C.C.L. McCrory, S. Jung, J.C. Peters, T.F. Jaramillo, Benchmarking heterogeneous electrocatalysts for the oxygen evolution reaction, J. Am. Chem. Soc. 135 (2013) 16977-16987.

[40]Y.F. Yuan, X.H. Xia, J.B. Wu, J.L. Yang, Y.B. Chen, S.Y. Guo, Nickel foam supported porous $Ni(OH)_2$/NiOOH composite film as advanced pseudocapacitor material, Electrochim. Acta 56 (2011) 2627-2632.